Research Article | Vol. 27, No. 6 | 18 Mar 2019 | OPTICS EXPRESS 7886
Optics EXPRESS

Reduction of laser-intensity-correlated noise in high-harmonic generation

MIKHAIL VOLKOV,* JUSTINAS PUPEIKIS, CHRISTOPHER R. PHILLIPS, FABIAN SCHLAEPFER, LUKAS GALLMANN, AND URSULA KELLER

Department of Physics, Institute of Quantum Electronics, ETH Zürich, 8093 Zürich, Switzerland
**volkovm@phys.ethz.ch*

Abstract: We present a scheme for correcting the spectral fluctuations of high-harmonic radiation. We show that the fluctuations of the extreme-ultraviolet (XUV) spectral power density can be predicted solely by monitoring the generating laser pulses; this method is in contrast with traditional balanced detection used in optical spectroscopy, where a replica of the signal is monitored. Such possibility emerges from a detailed investigation of high-harmonic generation (HHG) noise. We find that in a wide parameter range of the HHG process, the XUV fluctuations are dominated by a spectral blueshift, which is correlated to the near-infrared (NIR) driving laser intensity variation. Numerical simulations support our findings and suggest that non-adiabatic blueshift is the main source of XUV fluctuations. A straightforward post-processing of the XUV spectra allows for noise reduction and improved precision of attosecond transient absorption experiments. The technique is readily transferable to attosecond transient reflectivity and potentially to attosecond photoelectron spectroscopy.

1. Introduction

High-harmonic generation (HHG) of extreme-ultraviolet (XUV) and soft-x-ray radiation lies at the origin of attosecond spectroscopy [1–3]. HHG provides a temporal resolution and a photon energy range, which enable direct observations of element-specific electron dynamics on its natural timescale in atoms, molecules and solids [4–6]. However, the typical signal-to-noise ratio (SNR) of attosecond spectroscopy is much smaller than of optical spectroscopy for several reasons. For example, HHG typically requires high-energy sub-100-femtosecond pulses and hence working at low (~kHz) repetition rates where laser noise is higher than for high-repetition-rate systems. Additionally, the intrinsic properties of HHG lead to noise: it has low conversion efficiency [7], is highly sensitive to the carrier-envelope offset phase (CEP) [8,9] and is a highly nonlinear process. While optical femtosecond transient absorption can detect spectrally-resolved changes in optical density around 10 μOD and smaller already in the kHz range [10–12], XUV attosecond transient absorption can currently only resolve transmission changes of 10 mOD [13–16], thus limiting the range of materials and pump intensities to investigate. Moreover, the driving laser fluctuations may result in a timing jitter of the attosecond pulse emission, as demonstrated in the theoretical analysis of [17], and therefore contribute to the timing accuracy [4] of attosecond photoemission experiments. The low conversion efficiency of HHG can be counteracted by scaling the driving pulse energy together with the geometrical size of the setup [18], by increasing the laser repetition-rate [19], extending the pressure-length product [20] or by using shorter driving wavelength [21]. However, once enough photons are generated to overcome the detector dark noise, the HHG stability becomes the main issue. In this paper, we demonstrate a new approach to improving the signal-to-noise ratio in attosecond spectroscopy measurements.

Powerful techniques from optical spectroscopy can be, in principle, transferred to the attosecond-XUV domain. Shot-to-shot referencing is widely used in attosecond transient absorption and photoelectron/photoion spectroscopy [22–25]. A further SNR improvement can be achieved via balanced detection [26], i.e. single-shot referencing, which in principle

#351829 https://doi.org/10.1364/OE.27.007886
Journal © 2019 Received 16 Nov 2018; revised 28 Dec 2018; accepted 3 Jan 2019; published 4 Mar 2019

Optics EXPRESS

can completely eliminate the probe fluctuations up to the quantum limit. In this scheme, a reference replica of the probe beam is measured simultaneously with the main transient signal either with a photodiode [27] (i.e. spectrally-integrated) or with an additional spectrometer [11]. A direct, dual-beam implementation of a balanced detection for attosecond pulses is very challenging, because it requires a duration-preserving splitting of the XUV beam and a duplicate of an expensive and large XUV spectrometer. As an alternative referencing approach, the XUV-induced photocurrent on a metallic mirror can be used to monitor the XUV intensity [28], however, such technique gives no access to spectral intensity variations.

A number of studies considered the possible sources of HHG fluctuations. It was shown in [29], that the HHG yield is highly correlated with the ion yield. In [30], the possibility to infer the XUV spectrum from post-HHG laser photon counting and the correlation of the XUV yield and laser intensity was recently demonstrated. Indeed, the ionization rate determines the first step in HHG and is highly nonlinear with the laser field strength [31]. However, in another study [32], HHG in a waveguide configuration revealed no correlation between the input laser and XUV pulse energy fluctuation. Moreover, an earlier work [33] demonstrated that the magnitude of HHG fluctuations depends on laser intensity and photon energy, which may be a consequence of the spectrally-dependent phase matching.

Here we show, that this seemingly contrasting behavior may have a common origin based on the intensity-induced spectral shift of the high harmonic which is inherently connected to the plasma generated during the HHG process. We experimentally observe these shifts in a wide range of HHG parameters around the phase-matching optimum. Moreover, the resulting spectrally-integrated XUV pulse energy may be correlated positively, negatively or not at all to the laser intensity fluctuation. We support our observations with numerical simulations, which include macroscopic propagation effects of both laser and XUV pulses and suggest that the HHG fluctuation is primarily caused by a plasma-induced blueshift of the carrier wavelength. Additionally, we confirm the suggestion of [33] that the relative HHG fluctuation is minimized around the phase-matching conditions.

Our better understanding of the underlying physics then allows us to predict the HHG fluctuations by monitoring the noise of the input laser power on a shot-to-shot basis. A simple post-processing of the data then reduces intensity-related HHG fluctuations by a factor of 4. Finally, we combine this noise correlation correction with a digital version of lock-in data acquisition using a shutter in a realistic configuration of an attosecond transient absorption experiment which demonstrates the potential and practical limitations of the technique. Our results are readily transferable to attosecond transient reflectivity measurements and potentially, to other attosecond spectroscopic and imaging techniques.

2. Experiment

In our experiments, see Fig. 1, a commercial laser system (Femtolasers) delivers 25-fs, 1.5-mJ near-infrared (NIR) pulses centered at 780 nm at 1 kHz repetition rate. The system provides a root mean square (rms) CEP stability of 120 mrad. The laser pulses are further compressed in a double-filament setup. These pulses drive the attosecond pump-probe beamline. A detailed description can be found in [34]. We can configure the setup to generate attosecond pulse trains (APTs) or single-attosecond pulses (SAPs) with a polarization-gating technique. In this manuscript, we focus on spectrally broad APTs driven by 15-fs pulses and show that analogous results are obtained with SAPs. For the HHG, 190-μJ NIR pulses are focused onto a 2-mm-long noble gas target using a concave mirror with a 750-mm radius of curvature, yielding an estimated focal spot size of about 35 μm ($1/e^2$ radius). The pulse energy is controlled with a motorized iris aperture, and thus the spot size is calculated with truncated Gaussian beam focusing equations [35].

We record the XUV spectra simultaneously with the input laser energy fluctuations. The laser energy fluctuation is monitored on a shot-to-shot basis with a digital acquisition card (DAQ), similarly to [36]. A pre-amplified photodiode signal (in photovoltaic mode) is

Optics EXPRESS

stretched with a 100-kHz low-pass filter prior to digitization (BNC coupling via NI-2110, DAQ NI-6251) at 2 MHz. The data is acquired in a short time window, externally-triggered by the laser pulses, thus suppressing the low-frequency electronic noise. The ratio of dark-to-bright photodiode signal fluctuations is 4×10^{-2} rms. Simultaneously, we acquire a continuous sequence of XUV spectra at a maximum rate of 100 Hz (limited by the CCD readout time) with the first exposure triggered by the laser pulse. After each exposure, which integrates over several XUV pulses, the camera sends a voltage pulse ("readout event"), which is collected by the same DAQ card. Finally, a mechanical shutter is used for pump modulation and an additional photodiode for the timing diagnostics of the shutter opening in real transient absorption experiments [13]. The system can run in parallel with our active interferometric stabilization of the pump-probe delay, which is required for pump-probe experiments over longer time durations.

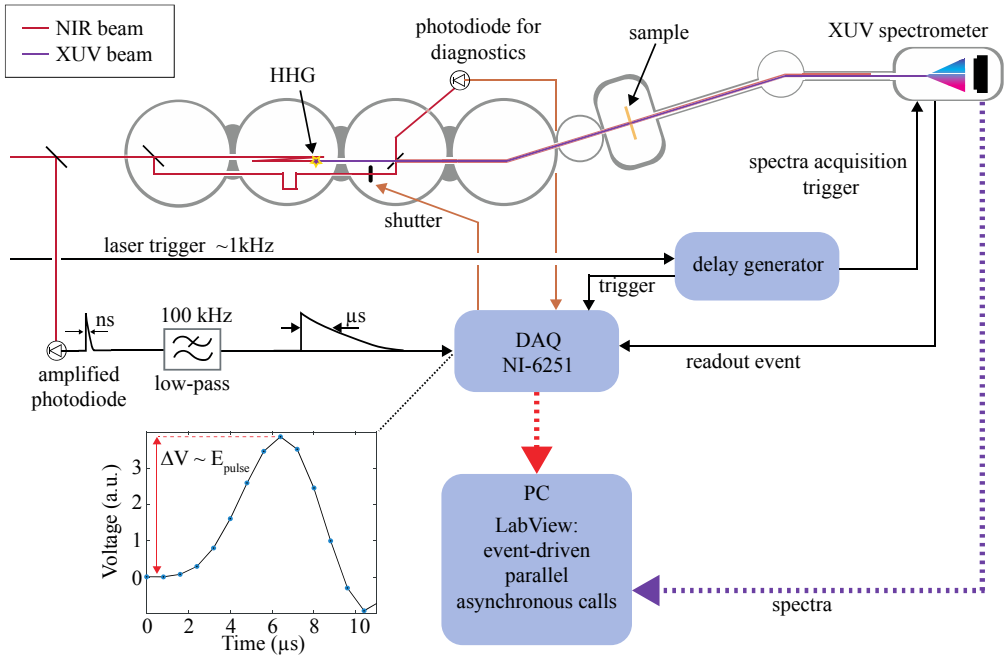

Fig. 1. Experimental setup. Attosecond pump-probe setup [34], combining the XUV spectral referencing (i.e. pump blocked with the shutter) with the correlation-correction technique. The laser pulse energy fluctuations are simultaneously recorded with the HHG spectra on a shot-to-shot basis with a DAQ card.

3. Results

3.1 Proof-of-principle demonstration

Figure 2(a) shows a typical HHG spectrum (blue line), generated in argon at 37 mbar with 15-fs pulses and averaged over 30 min of acquisition, consisting of ~3.6×10^4 spectra recorded with 50-ms exposure, i.e. averaged in a frequency band of 0.6 mHz to 20 Hz. The spectrometer resolution is limited by the CCD pixel size, resulting in a varying resolution from 20 meV at 25 eV to 160 meV at 65 eV. Note, that the XUV detection is not shot-noise limited. The number of XUV photons at the detector is directly calculated from the sensor quantum efficiency and the camera gain factor (electrons per digital count), yielding 1.75×10^5 photons per exposure, and therefore $\sigma_{shot} = 1/\sqrt{N} \approx 0.2\%$, where σ_{shot} is the standard deviation and N is the number of photons.

We find that the relative rms NIR intensity fluctuation of $\sigma^{NIR}/I^{NIR} = 0.5\%$ transfers into the XUV relative spectral power density fluctuation of $\sigma^{XUV}(\omega)/I^{XUV}(\omega) = 2$ - 20%, depending

Optics EXPRESS

on the photon energy. The standard deviation of the spectrum (red line) overlaid on Fig. 2(a) is notably different from the shape of the recorded spectrum. It implies that the XUV spectral fluctuations have a complicated character, which is not simply related to the fluctuation of the energy in each harmonic. We define variables "XUV_ω" as the XUV spectral density and "NIR" as the pulse energy of the driving laser. We may assume, that the spectrally-dependent fluctuations $\Delta(XUV_\omega)$ are caused by the laser energy fluctuations $\Delta(NIR)$ as well as other factors (CEP, gas pressure, beam pointing etc.), noted as ξ_n:

$$\Delta XUV_\omega \approx \frac{\partial XUV_\omega}{\partial NIR}\Delta NIR + \sum_n \frac{\partial XUV_\omega}{\partial \xi_n}\Delta\xi_n \qquad (1)$$

To determine the contributions from the first term in Eq. (1), we first note that the XUV spectra are acquired with a 50-ms exposure (50 shots), while the NIR energy is detected shot-to-shot. To compare them we, therefore, average the NIR energy over 50 shots. Given our measurement time of 30 minutes and the 50-ms XUV spectrometer exposure (20 Hz data acquisition rate) this yields a data series of length 3.6×10^4 for each resolved XUV photon energy. To illustrate the resulting data, we select an example photon energy around 39.6 and 40.3 eV in a 0.5 eV-wide band (orange and blue bars, Fig. 2(a)), and display the data on a scatter plot against the 50-ms-averaged NIR energy fluctuation, see Fig. 2(b). We find that the XUV and NIR fluctuations are highly correlated at these example photon energies. To quantify the correlation as a function of photon energy, for each resolved photon energy we perform a least-squares linear fit of the corresponding scatter plot, and model the slope of the fit c_ω as the spectral correlation $c_\omega = \partial XUV_\omega/\partial NIR$ (not to be confused with normalized covariance, i.e. the Pearson correlation coefficient).

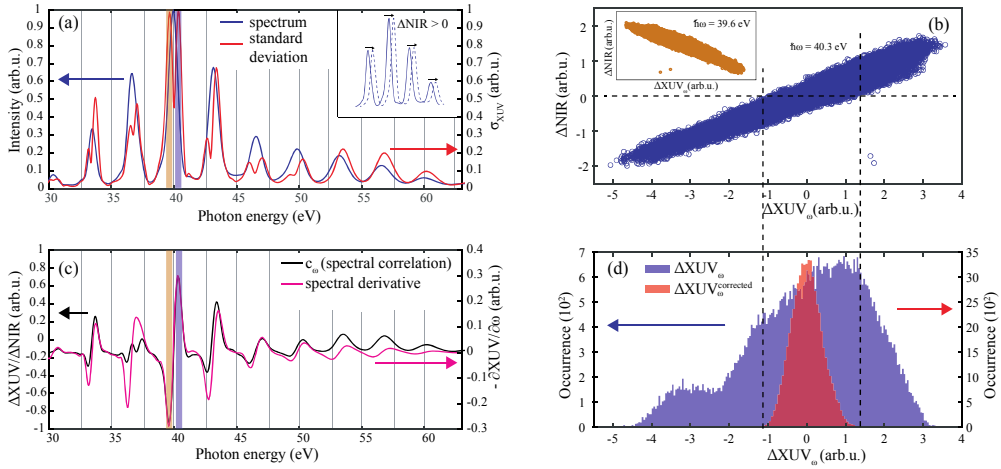

Fig. 2. (a) HHG spectrum generated in Ar with 15 fs pulses (blue line), overlaid with its standard deviation (red line). The inset depicts a spectral blueshift induced by a positive NIR intensity fluctuation, which causes the XUV fluctuation. (b) Scatter plot of NIR and XUV fluctuations in the photon energy bands of 40.1 to 40.6 eV and 39.4 to 39.9 eV, marked with a blue and orange bars in the panel "a", respectively. The inset shows anti-correlation corresponding to the photon energies selected with the orange bar. (c) Spectral correlation of intensity-induced XUV fluctuation (black line) extracted from a linear fit of the scatter plot for each photon energy independently. The overlaid pink line shows the negative derivative of the spectrum with respect to photon energy, which represents the effect of a small spectral blueshift. (d) Histograms of raw (blue) and balanced (red) XUV fluctuations in the same photon energy band. The width of the balanced histogram can be roughly estimated from the width of a constant-NIR section ($\Delta NIR = 0$) of the scatter plot (indicated with dashed lines).

Optics EXPRESS

Note, that the occurrence magnitude of the red histogram is much higher since all the XUV data is rescaled and not simply rejected.

By comparing the standard deviation (Fig. 2(a), red line) with the determined spectral correlation (Fig. 2(c), black line), we find that the standard deviation maxima coincide with the maxima/minima of the spectral correlation. This observation is consistent with NIR energy fluctuations being the dominant source of XUV noise, i.e.

$$\left|\frac{\partial XUV_\omega}{\partial NIR}\sigma_{NIR}\right| \gg \left|\sum_n \frac{\partial XUV_\omega}{\partial \xi_n}\sigma_{\xi_n}\right| \tag{2}$$

Next, we notice that the spectral noise correlation closely resembles the negative derivative of the spectrum with respect to photon energy (Fig. 2(c), pink line):

$$\frac{\partial XUV_\omega}{\partial NIR} \propto -\frac{\partial XUV}{\partial \omega} \tag{3}$$

i.e. the increase of the NIR intensity leads to a blue-shift of the XUV spectrum as a whole, see inset in Fig. 2(a).

Knowing the spectral noise correlation, it is, in principle, possible to predict the XUV fluctuations from the NIR intensity and improve the confidence interval up to the limit

$$\min\left|\Delta XUV_\omega^{corrected}\right| = \sum_n \left|\frac{\partial XUV_\omega}{\partial \xi_n}\Delta\xi_n\right| \tag{4}$$

determined by other noise contributions that are uncorrelated to the NIR fluctuation. The noise remaining in the post-processed XUV signal may be higher than the limit corresponding to Eq. (4) due to uncertainty of the NIR detection, e.g. electronic noise in the NIR detector. The noise correction level can be estimated from a section of the scatter plot at a fixed NIR value, see Fig. 2(b), dashed lines.

For a more accurate demonstration in our 30-min measurement, we correct each XUV data point as follows:

$$\Delta XUV_\omega^i = XUV_\omega^i - \overline{XUV}_\omega \tag{5}$$

$$\Delta XUV_\omega^{corrected,i} = \Delta XUV_\omega^i - c_\omega\left(NIR^i - \overline{NIR}\right) \tag{6}$$

where i numbers the individual XUV spectra, and the overline indicates the average value. Figure 2(d) shows the original (blue) and corrected (red) histograms of the XUV intensity (in the same photon energy band, marked in blue) with a factor of ~4 improvement.

3.2 Transient absorption configuration

Shot-to-shot referencing is widely used in current attosecond pump-probe experiments, usually by means of a chopper or shutter, which periodically blocks the pump beam to take the "reference" measurement. Therefore, in practice, the low-frequency noise below the shutter frequency is already suppressed. In our experiments, we use a fast (up to 50 Hz) water-cooled mechanical shutter. Faster chopping rates can be achieved with a tuning fork chopper [37]. However, the rate-limiting factor in transient absorption experiments comes from the spectrometer CCD readout time, which is around 8 ms in our case and can only be decreased at the expense of the SNR or the spectral span (e.g. by reducing the CCD readout region). To estimate the additional improvement attainable with the noise correlation correction as discussed above, we present in Fig. 3 the data from the scatter plot of Fig. 2(b) in the frequency domain. The reduction of XUV noise, shown as red vs blue lines in Fig. 3(a), is present for all resolved frequencies. To demonstrate the effect of correlation-correction in a

Optics EXPRESS

trial transient absorption configuration that was performed without an actual sample for the sake of generality, we choose the referencing (shutter) frequency to be 2.5 Hz ($f_{shutter}$, dashed line in Fig. 3(a)) and calculate the precision of the "transient" optical density in the standard way:

$$\Delta OD_i(\omega) = \ln \frac{XUV_\omega^i}{XUV_\omega^{i+1}} \tag{7}$$

where consecutive spectra XUV^i_ω and XUV^{i+1}_ω represent "reference" and "signal" spectra (NIR pump beam blocked and unblocked, respectively).

Figure 3(b) compares the distributions of optical density for the cases of uncorrected (blue) and corrected (red) data, exhibiting a factor of ~2 improvement. These results demonstrate that correlation-correction can be combined with shot-to-shot referencing to further improve the SNR. However, the degree of achievable improvement depends on the referencing speed.

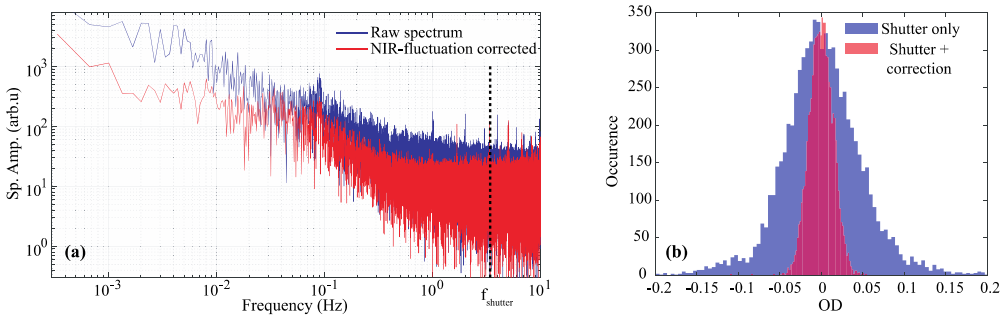

Fig. 3. (a) Spectral analysis of the corrected XUV fluctuations. Blue and red lines show the Fourier-amplitudes |FFT(XUV_ω)| of the raw and corrected XUV intensity in photon energy band of 40.1 to 40.6 eV. The dashed vertical line indicates the referencing (shutter) frequency. (b) Trial measurements of the accuracy of optical density determination (without actual sample), comparing the shutter-only measurement (blue histogram) with additional post-processing correction (red).

3.3 Microscopic origin of HHG fluctuations

To verify the robustness of the correlation, we investigate the spectral correlation coefficient for different experimental parameters. We support our observations with numerical simulations of HHG using the strong-field approximation (SFA) [38] with the ionization rates from the Perelomov-Popov-Terent'ev model (PPT) [31] including macroscopic propagation of the laser and generated XUV fields [39]. The diffraction operator is omitted for the XUV propagation, since its Rayleigh length (~40 mm) is much larger than the target length (2 mm). For comparison with experiment, we radially integrate the final XUV spectrum.

To determine the intensity-induced fluctuation, we vary the NIR power by 1% in the simulation and compute the difference $\Delta XUV_\omega^{simulated} = XUV_\omega(E^{NIR} + 0.01 \times E^{NIR}) - XUV_\omega(E^{NIR})$, where E^{NIR} is the input laser pulse energy. Figure 4 compares the experimental and theoretical HHG spectra together with the NIR-induced fluctuation as a function of the target offset from the geometrical focus. Both, in experiment and theory, the spectral blueshift can be observed as a function of the target position as well as due to NIR intensity fluctuation at a fixed target position. The spectral blueshift of high-harmonics with intensity was previously observed and discussed, e.g. in [40–42]. It could include both the self-action of the driving laser field due to plasma generation and the non-adiabaticity of the HHG process. We can estimate the plasma-induced self-frequency-shift of the NIR pulse by calculating the refractive change due to a 0.5% pulse energy increase which results in a 30 meV shift of harmonic order N = 30 at intensity of 1.7×10^{14} W/cm^2 in a 2-mm Argon cell. Thus this self-

Optics EXPRESS

frequency-shift alone can explain the experimentally observed 30 meV harmonic blue-shift at 0.5% pulse energy fluctuation.

In the experiment the pulse and beam do not correspond to an ideal Gaussian shape, we therefore determine the peak intensity from the experimental cutoff of 67 eV in HHG. This is well known to be more accurate. In the simulations, we used 175-μJ pulses of Gaussian shape and 15-fs duration, centered at 780 nm, focused into a 50-μm spot ($1/e^2$ radius, if focused in vacuum), and a 2-mm gas target filled with 50 mbar of argon. Given the uncertainty of the exact laser intensity distribution in the focus the agreement with theory is satisfactory.

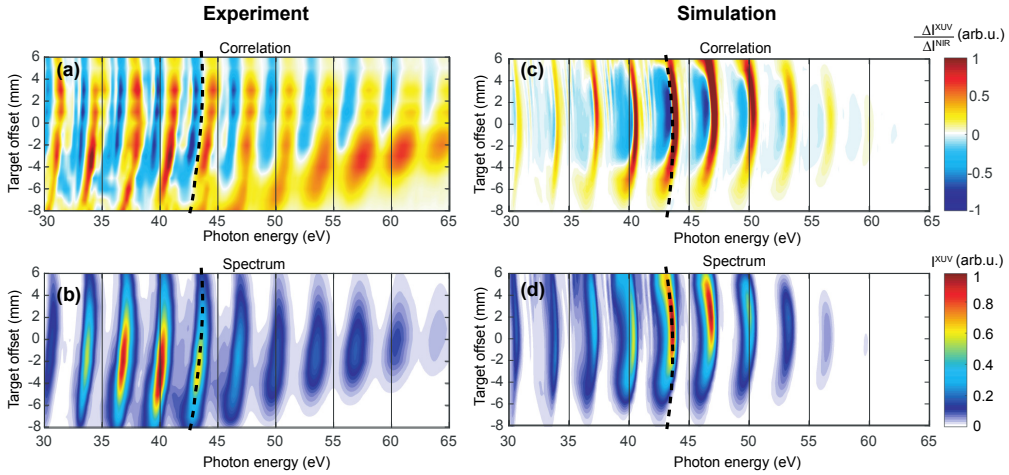

Fig. 4. Experiment (a), (b) and simulation (c), (d) showing the HHG spectrum and the pulse-intensity-induced fluctuation. Dashed curved lines indicate that the harmonic maxima correspond to the separation between blue (negative correlation) and red (positive correlation) regions of the correlation plots in the upper panels. In the simulation, the NIR intensity is varied by 1%, in the experiments the NIR rms is 0.5%.

Furthermore by scanning the experimental HHG parameters around the phase-matched optimum, we find that the blueshift remains the dominant contribution for the intensity-induced fluctuations. Specifically, by varying the intensity and gas pressure in the experiment, as shown in Figs. 5(a)-5(c), we find that the observed general character of correlation is robust against these parameters, although the total XUV counts may vary by an order of magnitude. However, the absolute scale of the correlation coefficient (upper panels in Fig. 4,5) varies much less with the target position, pressure and intensity compared to the XUV signal itself. Hence if we consider the relative XUV noise $\sigma^{XUV}(\omega)/I^{XUV}(\omega)$, the numerator is weakly dependent on HHG target conditions (Figs. 4(a) and 4(c)), while the denominator is strongly dependent on HHG target conditions (Figs. 4(b) and 4(d)). Hence the relative XUV noise can be minimized around the optimal phase-matching parameters since this maximizes $I^{XUV}(\omega)$. In addition, we find that the correlation of XUV and NIR fluctuations is present for all driving pulse durations from 5.5 to 25 fs, covering the regimes of APT generation as well as polarization-gated SAP generation, see Fig. 5(e).

Optics EXPRESS

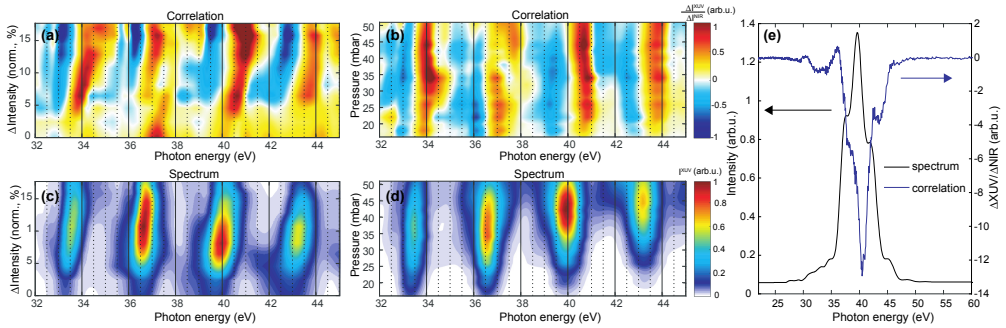

Fig. 5. Experimental HHG parameter scans, showing the intensity-induced spectral fluctuations and the corresponding spectra: (a, c) laser intensity and (b, d) gas pressure. (e) Single attosecond pulse (black line) generated by means of polarization-gating and the corresponding spectral correlation (blue).

4. Conclusion / outlook

We have investigated the noise properties of HHG and demonstrated a scheme for further noise reduction using the well-characterized energy-dependent NIR to XUV noise correlation. We measured a one-to-one mapping of small NIR laser pulse energy variations to the XUV spectrum. With this method, the SNR in experiments with HHG can be improved beyond shot-to-shot referencing. By comparing the experiments with numerical simulations, we have found that the non-adiabatic blueshift is the main origin of the laser-induced XUV variation.

We have demonstrated a combination of shot-to-shot referencing with correlation-correction in a transient absorption configuration. The extended sensitivity makes transient absorption applicable to more materials and wider pump intensity ranges. Our technique can be extended to any other possible type of XUV-NIR pump-probe spectroscopy, provided that other HHG parameters, such as the CEP, beam pointing and gas pressure are relatively stable. Several other methods to improve the SNR with the same setup could be implemented. For example, since most attosecond pump-probe experiments are driven by one laser source it is also possible to correct for the noise of the "pump" pulses. Our technique is readily transferable to attosecond transient reflectivity experiments. Moreover, the precision of attosecond photoelectron spectroscopy may be increased with the same technique, in particular, the sensitivity of the XUV spectral phase to the NIR intensity may be accounted for. The signal-to-noise problem will become even more severe in the soft-x-ray domain, with much lower generation efficiency and much higher harmonic orders. Correspondingly, in this domain, the demonstrated correlation-correction could be especially important. Finally, the laser-to-HHG spectral mapping can be transferred to high-harmonic generation in solids, possibly providing a better insight into its nature.

Funding

NCCR MUST, funded by the Swiss National Science Foundation (SNSF); SNSF (project 200020_172644).

Acknowledgments

We thank Benjamin Willenberg for assistance with setting up the spectrometer for continuous data collection mode and assistance with the numerical implementation of PPT ionization rates.

References

1. M. Ferray, A. L'Huillier, X. F. Li, L. A. Lompre, G. Mainfray, and C. Manus, "Multiple-harmonic conversion of 1064 nm radiation in rare gases," J. Phys. At. Mol. Opt. Phys. **21**(3), L31–L35 (1988).
2. A. McPherson, G. Gibson, H. Jara, U. Johann, T. S. Luk, I. A. McIntyre, K. Boyer, and C. K. Rhodes, "Studies

Optics EXPRESS

of multiphoton production of vacuum-ultraviolet radiation in the rare gases," J. Opt. Soc. Am. B **4**(4), 595 (1987).
3. P. M. Paul, E. S. Toma, P. Breger, G. Mullot, F. Auge, P. Balcou, H. G. Muller, and P. Agostini, "Observation of a train of attosecond pulses from high harmonic generation," Science **292**(5522), 1689–1692 (2001).
4. F. Krausz and M. Ivanov, "Attosecond physics," Rev. Mod. Phys. **81**(1), 163–234 (2009).
5. L. Gallmann, C. Cirelli, and U. Keller, "Attosecond science: recent highlights and future trends," Annu. Rev. Phys. Chem. **63**(1), 447–469 (2012).
6. F. Calegari, G. Sansone, S. Stagira, C. Vozzi, and M. Nisoli, "Advances in attosecond science," J. Phys. At. Mol. Opt. Phys. **49**(6), 062001 (2016).
7. V.-M. Gkortsas, S. Bhardwaj, E. L. Falcão-Filho, K.-H. Hong, A. Gordon, and F. X. Kärtner, "Scaling of high harmonic generation conversion efficiency," J. Phys. At. Mol. Opt. Phys. **44**(4), 045601 (2011).
8. H. R. Telle, G. Steinmeyer, A. E. Dunlop, J. Stenger, D. H. Sutter, and U. Keller, "Carrier-envelope offset phase control: A novel concept for absolute optical frequency measurement and ultrashort pulse generation," Appl. Phys. B **69**(4), 327–332 (1999).
9. A. Baltuška, T. Udem, M. Uiberacker, M. Hentschel, E. Goulielmakis, Ch. Gohle, R. Holzwarth, V. S. Yakovlev, A. Scrinzi, T. W. Hänsch, and F. Krausz, "Attosecond control of electronic processes by intense light fields," Nature **421**(6923), 611–615 (2003).
10. C. Schriever, S. Lochbrunner, E. Riedle, and D. J. Nesbitt, "Ultrasensitive ultraviolet-visible 20 fs absorption spectroscopy of low vapor pressure molecules in the gas phase," Rev. Sci. Instrum. **79**(1), 013107 (2008).
11. A. L. Dobryakov, S. A. Kovalenko, A. Weigel, J. L. Pérez-Lustres, J. Lange, A. Müller, and N. P. Ernsting, "Femtosecond pump/supercontinuum-probe spectroscopy: optimized setup and signal analysis for single-shot spectral referencing," Rev. Sci. Instrum. **81**(11), 113106 (2010).
12. F. Kanal, S. Keiber, R. Eck, and T. Brixner, "100-kHz shot-to-shot broadband data acquisition for high-repetition-rate pump-probe spectroscopy," Opt. Express **22**(14), 16965–16975 (2014).
13. F. Schlaepfer, M. Lucchini, S. A. Sato, M. Volkov, L. Kasmi, N. Hartmann, A. Rubio, L. Gallmann, and U. Keller, "Attosecond optical-field-enhanced carrier injection into the GaAs conduction band," Nat. Phys. **14**(6), 560–564 (2018).
14. H. Mashiko, Y. Chisuga, I. Katayama, K. Oguri, H. Masuda, J. Takeda, and H. Gotoh, "Multi-petahertz electron interference in Cr:Al_2O_3 solid-state material," Nat. Commun. **9**(1), 1468 (2018).
15. A. Moulet, J. B. Bertrand, T. Klostermann, A. Guggenmos, N. Karpowicz, and E. Goulielmakis, "Soft x-ray excitonics," Science **357**(6356), 1134–1138 (2017).
16. M. Zürch, H. T. Chang, L. J. Borja, P. M. Kraus, S. K. Cushing, A. Gandman, C. J. Kaplan, M. H. Oh, J. S. Prell, D. Prendergast, C. D. Pemmaraju, D. M. Neumark, and S. R. Leone, "Direct and simultaneous observation of ultrafast electron and hole dynamics in germanium," Nat. Commun. **8**, 15734 (2017).
17. C. Hernández-García, T. Popmintchev, M. M. Murnane, H. C. Kapteyn, L. Plaja, A. Becker, and A. Jaron-Becker, "Isolated broadband attosecond pulse generation with near- and mid-infrared driver pulses via time-gated phase matching," Opt. Express **25**(10), 11855–11866 (2017).
18. C. M. Heyl, C. L. Arnold, A. Couairon, and A. L'Huillier, "Introduction to macroscopic power scaling principles for high-order harmonic generation," J. Phys. At. Mol. Opt. Phys. **50**(1), 013001 (2017).
19. M. Krebs, S. Hädrich, S. Demmler, J. Rothhardt, A. Zaïr, L. Chipperfield, J. Limpert, and A. Tünnermann, "Towards isolated attosecond pulses at megahertz repetition rates," Nat. Photonics **7**(7), 555–559 (2013).
20. T. Popmintchev, M.-C. Chen, A. Bahabad, M. Gerrity, P. Sidorenko, O. Cohen, I. P. Christov, M. M. Murnane, and H. C. Kapteyn, "Phase matching of high harmonic generation in the soft and hard X-ray regions of the spectrum," Proc. Natl. Acad. Sci. U.S.A. **106**(26), 10516–10521 (2009).
21. D. Popmintchev, C. Hernández-García, F. Dollar, C. Mancuso, J. A. Pérez-Hernández, M.-C. Chen, A. Hankla, X. Gao, B. Shim, A. L. Gaeta, M. Tarazkar, D. A. Romanov, R. J. Levis, J. A. Gaffney, M. Foord, S. B. Libby, A. Jaron-Becker, A. Becker, L. Plaja, M. M. Murnane, H. C. Kapteyn, and T. Popmintchev, "Ultraviolet surprise: Efficient soft x-ray high-harmonic generation in multiply ionized plasmas," Science **350**(6265), 1225–1231 (2015).
22. M. Huppert, I. Jordan, and H. J. Wörner, "Attosecond beamline with actively stabilized and spatially separated beam paths," Rev. Sci. Instrum. **86**(12), 123106 (2015).
23. M. F. Jager, C. Ott, C. J. Kaplan, P. M. Kraus, D. M. Neumark, and S. R. Leone, "Attosecond transient absorption instrumentation for thin film materials: Phase transitions, heat dissipation, signal stabilization, timing correction, and rapid sample rotation," Rev. Sci. Instrum. **89**(1), 013109 (2018).
24. M. Lucchini, S. A. Sato, A. Ludwig, J. Herrmann, M. Volkov, L. Kasmi, Y. Shinohara, K. Yabana, L. Gallmann, and U. Keller, "Attosecond dynamical Franz-Keldysh effect in polycrystalline diamond," Science **353**(6302), 916–919 (2016).
25. A. Jain, T. Gaumnitz, A. Bray, A. Kheifets, and H. J. Wörner, "Photoionization delays in xenon using single-shot referencing in the collinear back-focusing geometry," Opt. Lett. **43**(18), 4510–4513 (2018).
26. H. P. Yuen and V. W. S. Chan, "Noise in homodyne and heterodyne detection," Opt. Lett. **8**(3), 177–179 (1983).
27. J. Brazard, L. A. Bizimana, and D. B. Turner, "Accurate convergence of transient-absorption spectra using pulsed lasers," Rev. Sci. Instrum. **86**(5), 053106 (2015).
28. C. Corder, P. Zhao, J. Bakalis, X. Li, M. D. Kershis, A. R. Muraca, M. G. White, and T. K. Allison, "Ultrafast extreme ultraviolet photoemission without space charge," Struct. Dyn. **5**(5), 054301 (2018).
29. B. D. Bruner, M. Krüger, O. Pedatzur, G. Orenstein, D. Azoury, and N. Dudovich, "Robust enhancement of high

Optics EXPRESS

harmonic generation via attosecond control of ionization," Opt. Express **26**(7), 9310–9322 (2018).
30. N. Tsatrafyllis, I. K. Kominis, I. A. Gonoskov, and P. Tzallas, "High-order harmonics measured by the photon statistics of the infrared driving-field exiting the atomic medium," Nat. Commun. **8**, 15170 (2017).
31. A. Perelomov, V. Popov, and M. Terent'ev, "Ionization of atoms in an alternating electric field," Sov. Phys. JETP **23**(5), 924 (1966).
32. S. J. Goh, Y. Tao, P. J. M. van der Slot, H. J. M. Bastiaens, J. Herek, S. G. Biedron, M. B. Danailov, S. V. Milton, and K.-J. Boller, "Single-shot fluctuations in waveguided high-harmonic generation," Opt. Express **23**(19), 24888–24902 (2015).
33. C. Erny, E. Mansten, M. Gisselbrecht, J. Schwenke, R. Rakowski, X. He, M. B. Gaarde, S. Werin, and A. L'Huillier, "Metrology of high-order harmonics for free-electron laser seeding," New J. Phys. **13**(7), 073035 (2011).
34. R. Locher, M. Lucchini, J. Herrmann, M. Sabbar, M. Weger, A. Ludwig, L. Castiglioni, M. Greif, M. Hengsberger, L. Gallmann, and U. Keller, "Versatile attosecond beamline in a two-foci configuration for simultaneous time-resolved measurements," Rev. Sci. Instrum. **85**(1), 013113 (2014).
35. H. Urey, "Spot size, depth-of-focus, and diffraction ring intensity formulas for truncated Gaussian beams," Appl. Opt. **43**(3), 620–625 (2004).
36. C. A. Werley, S. M. Teo, and K. A. Nelson, "Pulsed laser noise analysis and pump-probe signal detection with a data acquisition card," Rev. Sci. Instrum. **82**(12), 123108 (2011).
37. A. Ludwig, E. Liberatore, J. Herrmann, L. Kasmi, P. López-Tarifa, L. Gallmann, U. Rothlisberger, U. Keller, and M. Lucchini, "Ultrafast Relaxation Dynamics of the Ethylene Cation $C_{(2)}H_{(4)}^{+\cdot}$," J. Phys. Chem. Lett. **7**(10), 1901–1906 (2016).
38. M. Lewenstein, P. Balcou, M. Y. Ivanov, A. L'Huillier, and P. B. Corkum, "Theory of high-harmonic generation by low-frequency laser fields," Phys. Rev. A **49**(3), 2117–2132 (1994).
39. M. B. Gaarde, J. L. Tate, and K. J. Schafer, "Macroscopic aspects of attosecond pulse generation," J. Phys. At. Mol. Opt. Phys. **41**(13), 132001 (2008).
40. H. J. Shin, D. G. Lee, Y. H. Cha, K. H. Hong, and C. H. Nam, "Generation of Nonadiabatic Blueshift of High Harmonics in an Intense Femtosecond Laser Field," Phys. Rev. Lett. **83**(13), 2544–2547 (1999).
41. M. Geissler, G. Tempea, and T. Brabec, "Phase-matched high-order harmonic generation in the nonadiabatic limit," Phys. Rev. A **62**(3), 033817 (2000).
42. C. Altucci, R. Bruzzese, C. de Lisio, M. Nisoli, S. Stagira, S. De Silvestri, O. Svelto, A. Boscolo, P. Ceccherini, L. Poletto, G. Tondello, and P. Villoresi, "Tunable soft-x-ray radiation by high-order harmonic generation," Phys. Rev. A **61**(2), 021801 (1999).